Properties of the intermediately bound α-, β- and γ-excitons in ZnO:Cu

1998 J. Phys.: Condens. Matter 10 2007

(http://iopscience.iop.org/0953-8984/10/9/007)

J. Phys.: Condens. Matter **10** (1998) 2007–2019. Printed in the UK PII: S0953-8984(98)84730-9

Properties of the intermediately bound α-, β- and γ-excitons in ZnO:Cu

P Dahan†, V Fleurov†, P Thurian‡, R Heitz‡, A Hoffmann‡ and I Broser‡

† Beverly and Raymond Sackler Faculty of Exact Sciences, School of Physics and Astronomy, Tel Aviv University, Tel Aviv 69978, Israel

‡ Institut für Festkörperphysik der TU-Berlin, Hardenbergstrasse 36, 10623 Berlin, Germany

Received 28 May 1997, in final form 2 December 1997

Abstract. A microscopical model is proposed, describing the origin and properties of three closely spaced zero-phonon lines observed in the green Cu band in ZnO:Cu crystals labelled α, β and γ. These excitations are known to be formed by a charge-transfer reaction with hole bound states. These lines are shown to originate from an intermediately bound exciton of acceptor type, $(Cu^{(+)}(d^9 + e), h)$. This sort of exciton, in which both carriers are captured at intermediate-radius orbitals, results from the wurzite-type symmetry of the ZnO:Cu system. The electronic structure obtained for these three intermediately bound excitons enables us to explain their magneto-optic behaviour and to calculate their g-values.

Additionally, we determined the quantum efficiency of both intracentre and exciton transitions by using time-resolved and calorimetric absorption spectroscopy. While no $(Cu^{(+)}, h)$–$Cu^{(2+)}(^2T_2)$ luminescence is observed in ZnS, the exciton states in ZnO are purely radiative only to the ground state, $Cu^{(2+)}(^2T_2)$. The picture of an intermediately bound exciton explains the recombination channels and also makes clear the difference between copper states in the ZnS and ZnO systems.

1. Introduction

Copper is a prominent luminescence activator in II–VI compounds which gives rise to various luminescence and absorption bands in the visible and near-infrared spectral regions [1–8]. In ZnS, CdS and ZnO, there are two transitions with Cu^{2+} as the ground state—the intracentre $Cu^{(2+)}(^2T_2$–$^2E)$ transition and the Cu^{2+}–$(Cu^{(+)}, h)$ charge-transfer transition (see figure 1). Despite certain similarities, there are some striking differences between the spectral properties of copper in the sulphide compounds and in ZnO. Compared to the cases of ZnS and CdS, the three Cu^{2+} levels in ZnO are much deeper and have binding energies of 1.233 eV, 1.2 eV and 3.25 eV respectively [9, 10]. At the onset of the Cu^{2+} charge-transfer band, sharp resonances (usually called α-, β- and γ-ZPL (zero-phonon lines)) are observed and interpreted as $(Cu^{(+)}, h)$ states, where h stands for a hydrogen-like hole state (see figure 2).

The three zero-phonon lines, α, β and γ, of the green luminescence of copper in ZnO [13–17] present a puzzle. Experimentally it is quite clear that the α-, β- and γ-lines appear due to transitions between the ground $Cu^{(2+)}(^2T_2)$ and excited $(Cu^{(+)}, h)$ states of the impurity. Three ZPLs are positioned in an energy interval of 14 meV with a hole binding energy of about 380 meV. Therefore, it is impossible to identify these as hydrogen-like hole states of a Coulomb potential. Magneto-optic measurements show that these ZPLs are Kramers doublets with different and anisotropic g-factors.

0953-8984/98/092007+13$19.50

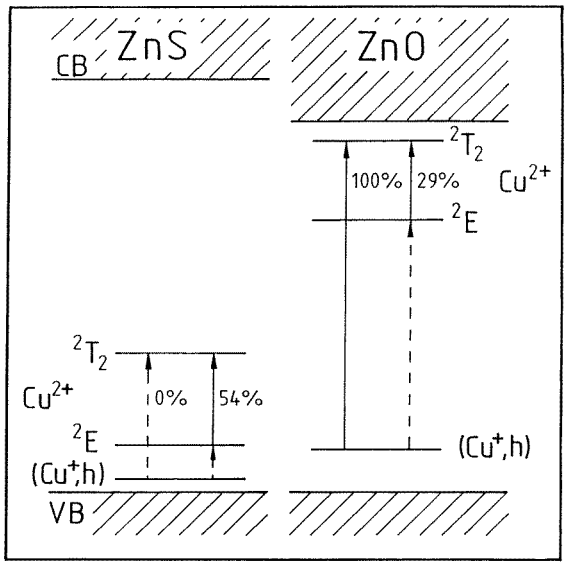

Figure 1. A schematic hole picture of copper in ZnO and ZnS. The $Cu^{2+}(^2E–^2T_2)$ and the $(Cu^+, h) \leftarrow Cu^{2+}$ transitions are represented by arrows. The dashed transitions are not observed in luminescence, and the calculated quantum yields η are also indicated.

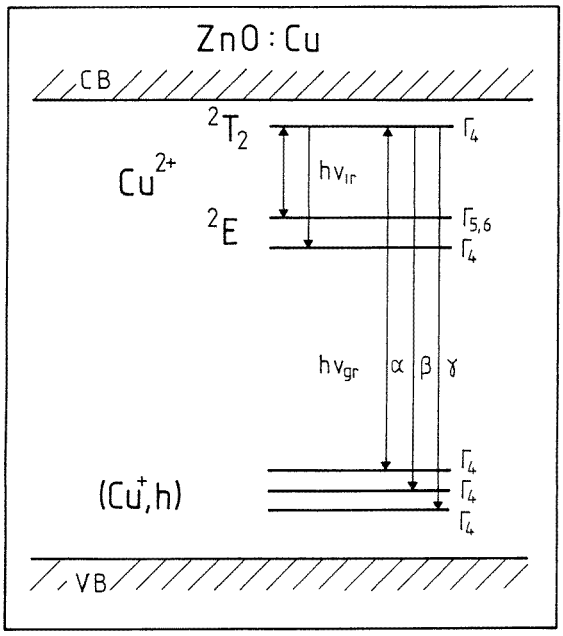

Figure 2. A schematic diagram of various transitions in ZnO:Cu in the hole representation, also exhibiting transitions providing the α-, β- and γ-lines.

It was shown [11, 12] recently for Ni in CdS that the approach based on deeply bound excitons may be not adequate and has to be modified for the wurzite-type crystals in order to

explain the experimental data. This has been done by means of the concept of intermediately bound excitons. The aim of this paper is to show that α-, β- and γ-ZPLs are connected to excitons intermediately bound to copper impurities, $[Cu^{(+)}(d^9 + e), h]$. The degree of localization of the tenth electron in copper and the binding energy and symmetry properties of the hole are considerably influenced by the symmetry of the crystalline environment of the impurity (the C_{3v} group). They are responsible for a significant change in the complex excitation spectra and other properties. The idea that the α-, β- and γ-ZPLs are due to excitation of the intermediately bound excitons is supported also by additional new experimental data on the isotope shifts of these ZPLs [18] and on their relaxation behaviour.

The relaxation behaviour of the excited (Cu^+, h) and $Cu^{2+}(^2E)$ states is studied by means of time-resolved spectroscopy allowing one to determine the radiative part of the relaxation and by calorimetric absorption spectroscopy (CAS) allowing one to determine the nonradiative part of the process. Using these data, calculations of the quantum efficiency for each transition can be carried out. It is shown that the decay of the excited $(Cu^{(+)}(d^9+e), h)$ states to the $Cu^{2+}(^2T_2)$ ground state is purely radiative. The picture of intermediately bound excitons explains this observation and makes clear the difference between the $Cu^{(+)}(d^{10}, h)$ states in ZnS and the intermediately bound exciton $(Cu^{(+)}(d^9 + e), h)$ states in ZnO.

2. Experimental results

2.1. The set-up

The samples used for the measurements are high-quality rods of ZnO grown in the laboratories of Professor Heiland, at Aachen, and Professor Mollwo, at Erlangen. The crystals contain copper as an unintentional dopant and the impurity concentration varies between 10 and 250 ppm. The copper concentration in the unintentionally doped ZnO crystals is determined by absorption measurements of the Cu^{2+} ZPL in combination with ESR measurements relative to a reference crystal with known copper concentration. The copper concentration of the reference crystal was analysed by chemical methods.

For the determination of radiative and nonradiative transition rates we combine data from the time-resolved photoluminescence experiments and CAS. CAS detects the increase of sample temperature caused by the generation of phonons during the nonradiative relaxation, and thus determines the quantum efficiencies η of the relaxation processes [19]. Using the time-resolved luminescence spectroscopy, we determine the lifetime τ of the excited states, which is limited by the radiative as well as by the nonradiative processes ($\tau^{-1} = W_r + W_{nr}$). The radiative and nonradiative relaxation rates are given by two parameters, τ and η:

$$W_r = \frac{\eta}{\tau} \qquad W_{nr} = \frac{1-\eta}{\tau}.$$

2.2. Results

Three ZPLs (α, β and γ) were detected in the excitation spectrum of the green Cu band in ZnO [14] and their binding energies were found to be rather close to each other. The Zeeman data for these lines have already been published by Broser *et al* [14] and Robbins *et al* [16] and the main results are briefly summarized here. All of the ZPLs exhibit anisotropic splitting with respect to the c-axis. The g-values of the different (Cu^+, h) states are presented in table 1. The anisotropies are different for the three transitions and thus the

recent new interpretation of the β- and γ-lines as local phonon modes of the α-transition, put forward by Mel'nichuk *et al* [17] is revised.

Table 1. Experimental and calculated g-values for α- β- and γ-ZPLs.

Line	Irreducible representation	Energy (eV)	$g_\parallel$		$g_\perp$	
			Experimental	Calculated	Experimental	Calculated
α	Γ_4	2.8602	2.2	1.85	−1.9	−2.15
β	Γ_4	2.8688	1.8	1.85	2.3	1.85
γ	Γ_4	2.8741	−2.0	−2.15	2.4	2.15

It is a striking fact that the luminescence intensity connected to the excited Cu^{2+} states in ZnO drastically differs from that in the sulphide compounds. In ZnS and CdS, intense infrared $Cu^{2+}(^2E–^2T_2)$ luminescence and absorption bands are easily observed, whereas the Cu^{2+} luminescence in ZnO is extraordinarily weak in spite of the strong absorption band.

Typical CAS spectra of Cu^{2+} in ZnO and ZnS have been published by Broser *et al* [20]. The results are summarized in figure 1. The quantum yields for the Cu^{2+} transitions are $\eta = 29 \pm 4\%$ for ZnO and $\eta = 54 \pm 4\%$ for ZnS. These quantum yields and the measured decay times, $\tau \approx 200$ ns for ZnO [21] and $\tau \approx 350$ ns for ZnS [22], enable us to calculate the radiative, W_r, as well as nonradiative, W_{nr}, rates for the Cu^{2+} transition. It was found that W_r is 1.5×10^6 s^{-1} for ZnO and ZnS, indicating the same oscillator strength. Additional efficient multiphonon relaxations with $W_{nr} = 3.6 \times 10^6$ s^{-1} for ZnO and 1.3×10^6 s^{-1} for ZnS take place.

The Cu^{2+} fine-structure spectra demonstrate that the $^2T_2$–^2E transition has a medium Huang–Rhys factor S. Thus, the multiphonon relaxation rate depends on the ratio between the transition and the phonon energies. A lower quantum yield η and a larger W_{nr} for Cu^{2+} can be understood as being results of the lower transition energy and the larger phonon energy in ZnO ($E_{LO(\gamma)} = 72.8$ meV (ZnO) or 42.8 meV (ZnS)). Hence, the Cu^{2+} luminescence intensity should be weaker for ZnO, but still observable.

Indeed, a resonant infrared excitation via the $^2T_2$–^2E absorption band leads to the detection of the Cu^{2+} luminescence in ZnO. However, a short-wavelength excitation of this luminescence using an Ar^+-ion laser or an XBO lamp as the excitation source is not successful for ZnO in contrast to ZnS. To resolve this problem, it is necessary to investigate different excitation processes and the corresponding transition rates in ZnS and ZnO.

Now we present a picture of the different excitation behaviours for the Cu^{2+} acceptor in ZnO and ZnS. In the sulphide compounds the Cu^{2+} luminescence can be efficiently excited above 1.2 eV via the acceptor-type charge-transfer process and the subsequent recapture of the free hole. The recombination of the acceptor (Cu^+, h) state into the $Cu^{2+}(^2E)$ state is essential for the excitation of the $Cu^{2+}(^2E–^2T_2)$ luminescence. This (Cu^+, h) state is observed in the PLE spectra of Cu^{2+} in ZnS. The proposed nonradiative decay of this state is supported by the quantum yield η of the (Cu^+, h)–$Cu^{2+}(^2T_2)$ process determined by means of CAS to be $0 \pm 2\%$. Furthermore, no (Cu^+, h)–$Cu^{2+}(^2T_2)$ luminescence is observed in ZnS (see figure 1).

The CAS and the calorimetric transmission spectra (CTS) of the (Cu^+, h)–Cu^{2+} transition in ZnO are shown in figure 3. Here, the energy difference between the (Cu^+, h) and the two Cu^{2+} states is much larger than for ZnS (figure 1), resulting in lower multiphonon recombination probabilities. Thus, the nonradiative recombination is completely quenched and the measured $8 \pm 4\%$ heat production (figure 3) is due solely to

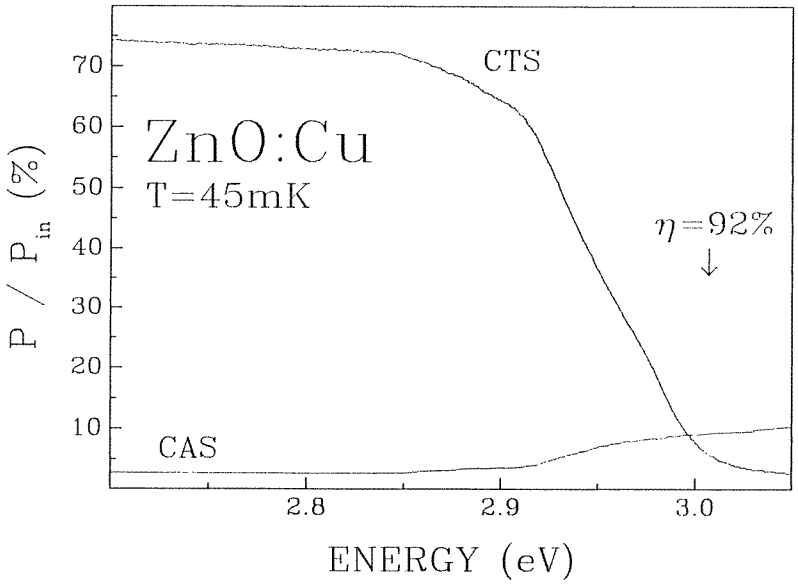

Figure 3. Calorimetric absorption and transmission spectra of the $(Cu^{+}, h) \leftarrow Cu^{2+}$ charge-transfer transition in ZnO at 45 mK. The calculated quantum yield η is $100 \pm 4\%$.

the phonon-assisted radiative recombination processes. In the photoluminescence spectra only the (Cu^{+}, h)–$Cu^{2+}(^2T_2)$ transitions are observed. Thus, the quantum yield of the green luminescence in ZnO is $100 \pm 4\%$. This proves that the $((Cu^{+}, h)$ state in crystals with less than 250 ppm copper concentration decays purely radiatively to the ground state since this process does not lead to an excitation of the $Cu^{2+}(^2E$–$^2T_2)$ luminescence. However, it should be remarked that larger copper concentrations usually quench the luminescence intensity. This is probably due to energy transfer between interacting copper centres or because of additional defects which open up additional nonradiative recombination channels. Our result is limited to the low-concentration regime, where only isolated copper centres have to be taken into account.

3. Theory

The model to be presented here assumes that the α-, β- and γ-ZPLs are associated with the $Cu^{+2}(d^9) + h\nu \rightarrow (Cu^{+}(d^{10}), h_i)$ transitions in which the Cu impurity in its ground state is excited in such a way that it binds an acceptor-type exciton. The tenth electron is bound to the impurity d shell in a state which is strongly swollen due to the covalent hybridization with the Bloch states of the host semiconductor. The exciton hole is captured by the potential created by this tenth electron. Mechanisms which may be responsible for this capture are discussed in our previous paper [12]. It is shown there that in hexagonal wurzite-type semiconductors the exciton electron may make a strong contribution to the impurity pseudopotential which has the properties of a projection operator and acts only on the Γ_4 states. This potential may create levels in the forbidden energy gap from the valence bands of the corresponding symmetry, since there are three valence bands with

their top wave functions transforming according to the Γ_4 irreducible representation†. in the hexagonal ZnO crystal one would expect to observe three levels in the forbidden energy gap which may be associated with the α-, β- and γ-ZPLs.

All of the mathematical details necessary for understanding this model are presented in reference [12]. Here this model will be briefly outlined and some details specific to the processes discussed in this paper will be added. The exciton electron wave function is looked for as an eigenstate of the electron Hamiltonian

$$H_e = \hat{T} + V_{\mathrm{d}}(\boldsymbol{r} - \boldsymbol{R}_0) + U'(\boldsymbol{r} - \boldsymbol{R}_0) \tag{1}$$

where $\hat{T}$ is the electron kinetic energy operator, $U'(\boldsymbol{r} - \boldsymbol{R}_0)$ is the lattice crystal-field potential acting on the transition metal impurity at the site $\boldsymbol{R}_0$ and $V_{\mathrm{d}}(\boldsymbol{r})$ is the d-impurity potential.

The electron wave function is expanded in the basis $\{\tilde{\psi}_{\boldsymbol{k}\mathrm{a}\sigma}, \psi_{\mathrm{d}\gamma\sigma}\}$ containing the impurity d orbitals, and the Bloch wave functions orthogonalized to these orbitals. Then the energy of the electron level within the forbidden energy gap is determined by the equation

$$E_{i\Gamma_1} = \varepsilon^{(10)}_{\Gamma_1} + M(E_{i\Gamma_1}) \tag{2}$$

where

$$M(E_{i\Gamma_1}) = \sum_{\mathrm{a}\boldsymbol{k}} \frac{|V_{\Gamma_5\mathrm{a}}(\boldsymbol{k})|^2}{E_{i\Gamma_1} - \varepsilon_{\mathrm{a}}(\boldsymbol{k})}. \tag{3}$$

and $V_{\Gamma_5\mathrm{a}}(\boldsymbol{k}) = \langle \mathrm{d}\Gamma_5|U'|\boldsymbol{k}\mathrm{a}\rangle$ is the matrix element responsible for the hybridization of the $\mathrm{d}\Gamma_5$ electron with Bloch state of the band a. The resulting bound electron states transform according to the irreducible representation Γ_5. However, accounting for the spin–orbit interaction (see, e.g., [23]) in the C_{3v} group, the Γ_5 state splits into several states with the Γ_4 ground state which will be of special interest to us in what follows.

The experimental position of this level in ZnO is about 0.2 eV below the bottom of the conduction band. Then the leading contribution to the mass operator $M(E_{i\Gamma_1})$ comes from the conduction band, hybridization with which is allowed in hexagonal crystals. Therefore, similarly to in the case of CdS:Ni discussed in references [11, 12], the electron wave function may be represented as a bonding combination

$$\psi^{(10)}_{i\Gamma_4} \simeq \frac{1}{\sqrt{(1 + M'_{\mathrm{c}\Gamma_4})}} \left[\psi_{\mathrm{d}} + \sqrt{M'_{\mathrm{c}\Gamma_4}}\varphi_{\mathrm{s}}\right] \tag{4}$$

in which the domination of the Bloch tail is ensured by the large value of

$$M'_{\mathrm{c}\gamma} = -\frac{\mathrm{d}M_{\mathrm{c}}(E_{i\gamma})}{\mathrm{d}E_{i\gamma}}$$

due to the proximity of the electron level to the conduction band c. These wave functions transform according to the irreducible representation Γ_4 and, as we will see below, determine also the symmetry properties of the bound hole states.

The hole wave function is an eigenfunction of the Hamiltonian

$$\left[-\left(\hat{T} + \sum_j U(\boldsymbol{r} - \boldsymbol{R}_i)\right) - U^{\mathrm{cc}} + \Delta\tilde{U} - E_{\mathrm{h}}\right]\psi_{\mathrm{b}\gamma}(\boldsymbol{r} - \boldsymbol{R}_0) = 0 \tag{5}$$

† It is worth mentioning here that the Γ_7 irreducible representation of the group C_{6v} describes these valence bands in pure wurzite crystals. A substitutional impurity lowers the point symmetry to C_{3v} and this irreducible representation becomes Γ_4. The irreducible representations of the point group C_{3v} will be used throughout the text.

where the analysis carried out in reference [12] allows one to keep just the pseudopotential

$$U^{\mathrm{cc}} = \left(\frac{M'_{\mathrm{a}\Gamma}}{1 + M'_{\mathrm{a}\Gamma}}\right)\hat{U}_{\mathrm{d}} \tag{6}$$

in which

$$\hat{U} = \Delta E\, \hat{P}_\Gamma + U_{\mathrm{d}}\hat{P}_\Gamma + \hat{P}_\Gamma U_{\mathrm{d}}$$

where $\hat{P}_\Gamma = |\varphi_\Gamma\rangle\langle\varphi_\Gamma|$ and φ_Γ is the Bloch tail of the impurity wave function (4), $\Delta E = E_{i\Gamma_4} - E_{\mathrm{h}}$. It appears due to the necessity of orthogonalizing the hole wave function to that of the tenth electron. The Coulomb interaction between the exciton electron and hole can be neglected here, or, if necessary, accounted for as a small perturbation [12]. Other contributions to the impurity potential are collected together in the short-range impurity $\Delta\tilde{U}$.

The calculation of the three hole Γ_4 levels is presented in appendix A; it leads to three equations for these levels, each of which is similar to a Slater–Koster equation (see, e.g., [23]). Sufficiently large values of M' such as can be expected in wurzite-type crystals allow one to obtain the three desired levels.

These levels are Γ_4 Kramers doublets originating from three Γ_4 valence bands. Calculating the corresponding wave functions in the same approximations leads to

$$\begin{aligned}
\psi^{(h)}_{\mathrm{b}\alpha}\left(+\frac{\tilde{1}}{2}\right) &= -\sin\frac{\theta}{2}\psi_{\mathrm{b,p}}\left|+\frac{\tilde{1}}{2}\right\rangle + \cos\frac{\theta}{2}\psi_{\mathrm{b,p'}}\left|+\frac{\tilde{1}}{2}\right\rangle \\
\psi^{(h)}_{\mathrm{b}\alpha}\left(-\frac{\tilde{1}}{2}\right) &= \sin\frac{\theta}{2}\psi_{\mathrm{b,p}}\left|-\frac{\tilde{1}}{2}\right\rangle - \cos\frac{\theta}{2}\psi_{\mathrm{b,p'}}\left|-\frac{\tilde{1}}{2}\right\rangle \\
\psi^{(h)}_{\mathrm{b}\beta}\left(+\frac{\tilde{1}}{2}\right) &= \cos\frac{\theta}{2}\psi_{\mathrm{b,p}}\left|+\frac{\tilde{1}}{2}\right\rangle + \sin\frac{\theta}{2}\psi_{\mathrm{b,p'}}\left|+\frac{\tilde{1}}{2}\right\rangle \\
\psi^{(h)}_{\mathrm{b}\beta}\left(-\frac{\tilde{1}}{2}\right) &= \cos\frac{\theta}{2}\psi_{\mathrm{b,p}}\left|-\frac{\tilde{1}}{2}\right\rangle + \sin\frac{\theta}{2}\psi_{\mathrm{b,p'}}\left|-\frac{\tilde{1}}{2}\right\rangle \\
\psi^{(h)}_{\mathrm{b}\gamma}\left(\pm\frac{\tilde{1}}{2}\right) &= \psi_{\mathrm{b,d}}\sqrt{\frac{2}{3}}\left[|\pm\tilde{1}\mp\rangle - \frac{1}{\sqrt{2}}|\tilde{0}\pm\rangle\right]
\end{aligned} \tag{7}$$

where

$$\tan\theta \simeq \frac{2\Delta_{\mathrm{p,p'}}}{\Delta_{\mathrm{p,p}} - \Delta_{\mathrm{p',p'}}}.$$

These functions are combinations of the pseudo-wave functions $\psi^{(\mathrm{h})}_{\mathrm{b,a}}$ each of which contains the contribution of only one of three valence bands, $\mathrm{a} = \mathrm{p}, \mathrm{p}'$ and d. The ket vectors $|\tilde{L}\sigma\rangle$ show the values of the reduced angular momentum and spin. The totally quenched momentum $\tilde{L} = 0$ for α and β is omitted.

Taking into account also the core part of the hole wave function constructed from the $\mathrm{Cu}(\tilde{\mathrm{d}}^{10})$ states, the full hole wave function (cf., equation (32) in [12]) is

$$\psi^{(\mathrm{h})}_i = \psi_{\mathrm{b}i} + F^{\gamma}_{\mathrm{d}}\psi_{\mathrm{d}\gamma_4}(\mathrm{Cu}) \tag{8}$$

where

$$F^{\gamma_4}_{\mathrm{d}} = \frac{\langle\gamma_4|W|\psi_{\mathrm{b}}\rangle}{E_i + E_{\gamma_4}}$$

and $i = \alpha, \beta, \gamma$.

These are three Γ_4 Kramers doublets corresponding to the α-, β- and γ-lines.

4. Optical properties

4.1. Magneto-optic behaviour

This section presents a comparison between the theoretical predictions and experimental observations for the magneto-optic behaviour of the α-, β- and γ-ZPLs. A magnetic field acts mainly on the hole, since the closed Cu(d^{10}) shell with its Γ_1 symmetry is hardly affected by the field. The spin Hamiltonian describing the linear Zeeman interaction in each Kramers doublet is generally written as

$$\mathcal{H}_Z = \mu_0(\gamma_r K \boldsymbol{L} + g_0 \boldsymbol{S}) \cdot \boldsymbol{H} \tag{9}$$

where $\boldsymbol{S}$ and $\boldsymbol{L}$ are the spin and orbital angular moments of the hole. The covalency reduction factor K is different for each hole state and will be found explicitly as a function of the hybridization parameter F_γ, equation (8). γ_r is the reduction factor due to the Ham effect [24].

The orbital angular moments of the p-type hole states corresponding to the Kramers doublets of α and β type are completely quenched, $\boldsymbol{L} = 1 \rightarrow \tilde{\boldsymbol{L}} = 0$ (a spin-like hole), due to the fact that the hole is bound by a short-range potential [25]. The γ-exciton hole has a d-type wave function with the reduced angular moment $\tilde{L} = 1$ in covalent crystals. Therefore, the effective spin Hamiltonian for each doublet $\tilde{J} = \frac{1}{2}$ in axial symmetry is

$$\mathcal{H}_Z = g_{\parallel eff} H_z \tilde{J}_z + g_{\perp eff}(H_x \tilde{J}_x + H_y \tilde{J}_y) \tag{10}$$

where

$$\begin{aligned} g_{\parallel eff} &= 2(g_s + g_{\tilde{L}})\left\langle i, \pm\frac{\tilde{1}}{2}\middle|\tilde{J}_z\middle|i, \pm\frac{\tilde{1}}{2}\right\rangle \\ g_{\perp eff} &= (g_s + g_{\tilde{L}})\left\langle i, \pm\frac{\tilde{1}}{2}\middle|\tilde{J}_+\middle|i, \mp\frac{\tilde{1}}{2}\right\rangle. \end{aligned} \tag{11}$$

g_s and g_L are calculated for the parallel and the perpendicular field configurations by projecting $\boldsymbol{S}$ and $\tilde{\boldsymbol{L}}$ onto the hole total angular momentum, $\boldsymbol{J}$:

$$\begin{aligned} g_s &= g_0 \frac{\boldsymbol{S}\cdot\boldsymbol{J}}{\boldsymbol{J}\cdot\boldsymbol{J}} \\ g_{\tilde{L}} &= \alpha\gamma_r \frac{\tilde{\boldsymbol{L}}\cdot\boldsymbol{J}}{\boldsymbol{J}\cdot\boldsymbol{J}} \end{aligned}$$

where $\boldsymbol{J} = \tilde{\boldsymbol{L}} + \boldsymbol{S}$. The covalency factor is $\alpha_{\mathrm{d}} = -1$ for a d-wave function and $\alpha_{\mathrm{p}} = 1$ for a p-wave function [26].

Using equation (10) and the hole wave functions (8) one gets

$$\begin{aligned} g_\parallel(\alpha,\beta) &= \left[g_0 - \frac{F_\gamma^2}{3}(g_0 - 4\gamma_r^{\mathrm{d}}\alpha)\right] + \Delta g_L \\ g_\parallel(\gamma) &= \left[-\frac{1}{3}(g_0 - 4\gamma_r^{\mathrm{b}}\alpha) - \frac{F_\gamma^2}{3}(g_0 - 4\gamma_r^{\mathrm{d}}\alpha)\right] + \Delta g_L \end{aligned} \tag{12}$$

and

$$g_\perp(\alpha) = \left[-g_0 - \frac{1}{3}(g_0 - 4\gamma_r^{\mathrm{d}}\alpha)F_{\gamma_4}^2\right] + \Delta g_L$$
$$g_\perp(\beta) = \left[g_0 - \frac{1}{3}(g_0 - 4\gamma_r^{\mathrm{d}}\alpha)F_{\gamma_4}^2\right] + \Delta g_L \tag{13}$$
$$g_\perp(\gamma) = \left[-\frac{1}{3}(4\gamma_r^{\mathrm{b}}\alpha - g_0) - \frac{F_\gamma^2}{3}(4\gamma_r^{\mathrm{d}}\alpha - g_0)\right] + \Delta g_L.$$

This type of hole bound with a considerably enhanced energy loses its host-state character and, hence, its behaviour is probably a spin-like one which means that $g_0 = +2$.

Here a distinction is made between the two reduction factors resulting from the interaction of the localized phonons with the hole wave function (8). The reduction factor γ_r^{b} results from the interaction with the band states and γ_r^{d} from the interaction with the d states of the Cu impurity. It was shown by Yamaguchi and Kamimura [27] that the reduction factor γ_r^{d} is about 0.65 due to the ground state of ZnO:Cu. Since the Bloch tail $\psi_{i\mathrm{b}}$ of the hole wave function formed by the band states weakly interacts with the local vibration modes, γ_r^{b} is estimated to be close to one. Using also a reasonable value for the hole hybridization matrix elements $F_{\gamma_4}^2 \approx 0.1$, we calculated the g-values which are presented in table 1.

One can see that all of the absolute values obtained for the g-factors are close to 2. This corresponds to the spin-like character of the hole bound with a relatively large binding energy, meaning that $g_0 = +2$. One can see that the calculated and measured g-values are rather close to each other and, what is more important, their signs coincide. A certain numerical misfit may be caused by our limited knowledge of the Δg_L correction. A more detailed knowledge of the hole wave function structure is also necessary.

4.2. Recombination channels

One of the important questions concerning the recombination channels for the α-, β- and γ-excitons is why the recombination goes only via the ground state $^2\mathrm{T}_2$ of the Cu^{2+} in ZnO, whereas, in other systems, acceptor excitation may also involve the excited state $^2\mathrm{E}$ of the impurity. In order to find out which of these two states plays the more important part in these recombination processes, we compare the corresponding rates of the radiative dipole transitions.

The intensity of a dipole transition is given by

$$I = \frac{4e^2\pi^2\nu^4}{c^3}|X_{if}|^2 \tag{14}$$

where the dipole matrix elements for the transitions between the bound exciton and the Cu (d^9) final states are

$$X_{if} = \langle\Psi_{f\Gamma}(\mathrm{d}^9)|\hat{\boldsymbol{R}}|\Psi_{\Gamma_4}^{(ex)}\rangle. \tag{15}$$

The exciton wave function is

$$\Psi_{\Gamma_4}^{(ex)} = \hat{A}\left(\frac{G_{\mathrm{T}_2}^{\mathrm{A}_1}}{\sqrt{3}}\Psi_{\mathrm{T}_2\Gamma_4}(\mathrm{d}^9)\psi_{\mathrm{t}_2\Gamma_4} + \frac{G_{\mathrm{E}}^{\mathrm{A}_1}}{\sqrt{2}}\Psi_{\mathrm{E}\Gamma_{5,6}}(\mathrm{d}^9)\psi_{\mathrm{e}\Gamma_{5,6}}\right)\psi_{i\Gamma_4}^{(\mathrm{h})} \tag{16}$$

and the Cu(d^9) wave functions are

$$\Psi_{f\Gamma_4} = \Psi_{\mathrm{T}_2\Gamma_4}(\mathrm{d}^9) \qquad \text{or} \qquad \Psi_{\mathrm{E}\Gamma_4}(\mathrm{d}^9). \tag{17}$$

Possible differences in the wave functions $\psi^{(h)}_{i\Gamma_4}$ for α-, β- or γ-excitons are of minor importance for this calculation.

The ratio of the recombination intensities, I_{t_2} and I_e, for the $^2T_2$ and ^2E states is calculated according to

$$\rho = \frac{I_{t_2}}{I_e} = \frac{2}{3}\left(\frac{G^{A_1}_{T_2}}{G^{A_1}_{E}}\right)^2\left(\frac{\nu_{t_2}}{\nu_e}\right)^4\left(\frac{M'_{t_2}}{M'_e}\right)\left(\frac{1+M'_e}{1+M'_{t_2}}\right)\left(\sum_i R_i\right)\Big/ R_z \tag{18}$$

where $R_i = |\langle\psi^{(h)}_{i\Gamma_4}|\hat{R}_i|\varphi_\gamma\rangle|^2$. γ is s for the transition to the state $^2T_2$ and p for that to the ^2E state; i takes the values x, y and z.

The value M'_{t_2} is expected to be large due to the position of $^2T_2$ level near the conduction band, while the ^2E level lying about 1 eV below the bottom of the conduction band should result in a small value of $M'_e \sim 0.15$. This difference reflects the corresponding difference in the localization radii of the impurity d electron in these two states, the radius in the ground state of the impurity being much larger than in the excited states. That is why the transition to the ground state has a much stronger intensity (cf., the antenna effect considered by Rashba and Gurgenishvili [28]).

Another contribution results from the fact that in the point group C_{3v}, recombination to the ^2E state is allowed only if z-polarized light is emitted with the corresponding dipole matrix element R_z, while recombination to the $^2T_2$ state is allowed for unpolarized light as well. The ratio of the photon frequencies $(\nu_{t_2}/\nu_e)^4$ should be also taken into account. As a result the I_e-intensity is expected to be about two orders of magnitude smaller than the I_{t_2}-intensity. This difference explains why only the recombination to the ground state $^2T_2$ is observed.

5. Summary

A microscopical model accounting for three close ZPLs, α, β and γ, in ZnO is proposed. The model addresses the origin of the excitations responsible for the appearance of these lines and various spectroscopic and optical features observed experimentally. Excitons intermediately bound to Cu impurities are the principal players. Excitons of this type can be formed in crystals with hexagonal wurzite-type lattices [11, 12] which is typical for ZnO. We have seen that the wave function of the rather loosely bound tenth electron in the Cu($\tilde{d}^{(10)}$) pseudo-ion is strongly swollen due to hybridization of the d states with the states at the bottom of the conduction band. On the other hand the hole wave function was found to be constructed by an admixture of the band states to the d states due to a nonlocal potential and strong orthogonalization corrections.

The dominant potential responsible for hole binding is a short-range pseudopotential with properties of a projection operator projecting onto the Γ_4 subspace. That is why this potential is capable of binding only holes from the valence bands of Γ_4 symmetry and this explains the origin of these three Kramers doublets.

It should be pointed out that in the case of Cu in CdS (wurzite), the intermediately bound exciton cannot be formed because of the mid-gap position of the $Cu^{2+/+}$ charge-transfer level [29], i.e., far away from the divergency of the function $M'_{c\gamma}$.

Using the concept of intermediately bound excitons, we are also able to explain the magneto-optic behaviour of the α-, β- and γ-ZPLs.

The extremely strong differences between two possible recombination channels of the α-, β- and γ-excitation states is explained using the concept of intermediately bound excitons. The exciton states, in various systems, are known to recombine to the ^2E and $^2T_2$ states of

the $Cu^{2+}(d^9)$ impurity, whereas in the case of the ZnO system the recombination is observed to the $^2T_2$ state only. This difference follows directly from the wave-function properties of the intermediately bound excitons.

The relaxation behaviour of the excited (Cu^+, h) and $Cu^{2+}(^2E)$ states is obtained by means of time-resolved spectroscopy used to determine the radiative relaxation and by CAS which determines the nonradiative recombination part. These data allow one to calculate the quantum efficiency for each transition. It is shown that the decay of the excited $(Cu^{(+)}(d^9 + e), h)$ states is purely radiative to the $Cu^{2+}(^2T_2)$ ground state. The picture of intermediately bound excitons explains this observation and makes clear the difference between the $Cu^{(+)}(d^{10}, h)$ states in ZnS and the intermediately bound exciton $(Cu^{(+)}(d^9 + e), h)$ states in ZnO.

Acknowledgment

We are indebted to the German–Israeli Foundation for Research and Development for support under grant No G-0456-220.07/95.

Appendix A. Hole levels

The pseudopotential (6) has the properties of a projection operator acting only on the functions transforming according to the Γ_4 irreducible representation. That is why this potential may form bound hole states only from the wave functions of three, a = p, p′ and d, valence bands constructed from p and d states, respectively [30, 31], and transforming according to the Γ_4 representation. Therefore just three hole levels corresponding to the α-, β- and γ-lines may appear.

The energies of these levels may be calculated using the same procedure as in [12], which uses the fact that the short-range potential (6) contains factorizable terms. The hole wave function is considered as an expansion:

$$\psi_{\mathrm{h}} = \sum_{k\mathrm{a}} F^{\Gamma_4}_{k\mathrm{a}} \tilde{\psi}_{k\mathrm{a}} \tag{A1}$$

over the orthogonalized Bloch states $\tilde{\psi}_{k\mathrm{a}}$. The summation is over the three above-mentioned valence bands, a = p, p′ and d. Then the quantities

$$\begin{aligned} A_{\mathrm{a}S} &= \sum_{k} S_{k\mathrm{a}\Gamma_4} F^{\gamma}_{k\mathrm{a}} \\ A_{\mathrm{a}V} &= \sum_{k} V_{k\mathrm{a}\Gamma_4} F^{\gamma}_{k\mathrm{a}} \end{aligned} \tag{A2}$$

are defined where $S_{k\mathrm{a}\Gamma_4} = \langle k\mathrm{a}\sigma|\tilde{\mathrm{d}}\Gamma_4\rangle$ and $V_{k\mathrm{a}\Gamma_4} = \langle k\mathrm{a}\sigma|V_{\mathrm{d}}|\tilde{\mathrm{d}}\Gamma_4\rangle$. The summation over k and the symmetry properties of the Bloch wave functions make these quantities real. The same simplifying approximation, $V_{k\mathrm{a}\Gamma_4} = VS_{k\mathrm{a}\Gamma_4}$, as was used in [12] is used here, where V is a parameter characterizing the impurity potential.

Substituting equation (A1) for the hole wave function into the Schrödinger equation (5) and then multiplying it by $S^*_{k\mathrm{a}}$ and summing over k produces three linear equations for the quantities (A2), namely:

$$A_{\mathrm{a}S} - \sum_{\mathrm{a}'} \left[B_{\mathrm{a}S S}(\Delta E + 2V) + \Delta_{\mathrm{a},\mathrm{a}'} \right] A_{\mathrm{a}'S} = 0 \tag{A3}$$

where a = p, p′ and d; and

$$B_{\mathrm{a}SS}(E_{\mathrm{h}}) = \frac{M'_{\mathrm{c}\Gamma}}{1+M'_{\mathrm{c}\Gamma}} \sum_{\boldsymbol{k}} \frac{1}{E_{\mathrm{a}\boldsymbol{k}} - E_{\mathrm{h}}} S^{*}_{\boldsymbol{k}\mathrm{a}\Gamma_4} S_{\boldsymbol{k}\mathrm{a}\Gamma_4}.$$

Equation (A3) also contains a contribution due to the short-range potential $\Delta\tilde{U}$ which is approximately represented as

$$\sum_{\boldsymbol{k},\boldsymbol{k}'} \frac{S^{*}_{\boldsymbol{k}\mathrm{a}\Gamma_4}}{E_{\mathrm{a}\boldsymbol{k}} - E_{\mathrm{h}}} \Delta U_{\mathrm{a,a}'}(\boldsymbol{k},\boldsymbol{k}') F^{\gamma}_{\boldsymbol{k}'\mathrm{a}'} \approx B_{\mathrm{a}SS}(E_{\mathrm{h}}) \sum_{\mathrm{a}'} \Delta_{\mathrm{a,a}'} A_{\mathrm{a}'S} \tag{A4}$$

where $\Delta U_{\mathrm{a,a}'}(\boldsymbol{k},\boldsymbol{k}')$ are the matrix elements of $\Delta\tilde{U}$.

Although the symmetry allows for mixing between all three valence bands, it should be rather strong between the p and p′ bands and weak if the d band is involved. That is why the matrix elements Δ_{dp} and $\Delta_{\mathrm{dp}'}$ will be neglected below:

$$\begin{vmatrix} 1-(X+\Delta_{\mathrm{dd}})B_{\mathrm{d}SS} & -XB_{\mathrm{d}SS} & -XB_{\mathrm{d}SS} \\ -XB_{\mathrm{p}SS} & 1-(X+\Delta_{\mathrm{pp}})B_{\mathrm{p}SS} & -(X+\Delta_{\mathrm{pp}'})B_{\mathrm{p}SS} \\ -XB_{\mathrm{p}'SS} & -(X+\Delta_{\mathrm{pp}'})B_{\mathrm{p}'SS} & 1-(X+\Delta_{\mathrm{p}'\mathrm{p}'})B_{\mathrm{p}'SS} \end{vmatrix} = 0 \tag{A5}$$

where X is standing for $\Delta E + 2V$ in this expression.

Equation (A5) without short-range potential matrix elements was studied in reference [12] and a level for the hole was found. In the general case, three hole levels may appear, equations for which may be found, for example, in the limit of large values of these matrix elements:

$$B_{\mathrm{d}SS} = \frac{1}{\Delta_{\mathrm{dd}}} \tag{A6}$$

$$B_{\mathrm{p}SS} = \frac{\Delta_{\mathrm{pp}} + \Delta_{\mathrm{p}'\mathrm{p}'}}{2D_{\mathrm{pp}'}} \pm \frac{\sqrt{(\Delta_{\mathrm{pp}} + \Delta_{\mathrm{p}'\mathrm{p}'})^2 - D_{\mathrm{p}'\mathrm{p}}}}{2D_{\mathrm{p}'\mathrm{p}}} \tag{A7}$$

where $D_{\mathrm{p}'\mathrm{p}} = \Delta_{\mathrm{pp}}\Delta_{\mathrm{p}'\mathrm{p}'} - \Delta^2_{\mathrm{pp}'}$. In order to avoid overcomplicated equations, we assume here that $B_{\mathrm{p}SS} = B_{\mathrm{p}'SS}$.

References

[1] Broser I and Broser-Warminsky R 1958 *J. Phys. Chem. Solids* **6** 386
[2] Broser I and Broser-Warminsky R 1962 *Luminescence of Organic and Inorganic Materials* (New York: Wiley) p 402
[3] Schulz H-J 1963 *Phys. Status Solidi* **3** 2117
[4] Shionoya S, Koda T, Era K and Fujiwara H 1964 *J. Phys. Soc. Japan* **19** 1157
[5] Solbrig C 1968 *Z. Phys.* **211** 429
[6] Era K, Shionoya S, Washizawa Y and Okamatsu H 1968 *J. Phys. Chem. Solids* **29** 1827
[7] Suzuki A and Shionoya S 1971 *J. Phys. Soc. Japan* **31** 1455
[8] Tabei M and Shionoya S 1977 *J. Lumin.* **15** 201
[9] Heitz R, Hoffmann A, Thurian P and Broser I 1992 *J. Phys. C: Solid State Phys.* **4** 157
[10] Godlewski M and Swiatek K 1992 *J. Cryst. Growth* **117** 634
[11] Dahan P, Fleurov V N and Kikoin K A 1995 *Mater. Sci. Forum* **196–201** 755
[12] Dahan P, Fleurov V N and Kikoin K A 1997 *J. Phys. C: Solid State Phys.* **9** 5355–70
[13] Dingle R 1969 *Phys. Rev. Lett.* **23** 579
[14] Broser I J and Rudolf K F 1978 *Solid-State Electron.* **21** 1597
[15] Dean P J, Robbins D J, Bishop S G, Savage J A and Porteous P 1981 *J. Phys. C: Solid State Phys.* **14** 2847
[16] Robbins D J, Herbert D C and Dean P J 1981 *J. Phys. C: Solid State Phys.* **14** 2859

[17] Mel'nichuk S V, Sokolov V I, Surkova T P and Chernov V M 1991 *Sov. Phys.–Solid State* **33** 1833
[18] Dahan P, Fleurov V N, Thurian P, Heitz R, Hoffmann A and Broser I 1998 *Phys. Rev.* B **57** at press
[19] Podlowski L, Hoffmann A and Broser I 1992 *J. Lumin.* **53** 359
[20] Broser I, Podlowsky L, Thurian P, Heitz R and Hoffmann A 1994 *J. Lumin.* **60+61** 588
[21] Kimpel B M and Schulz H-J 1991 *Phys. Rev.* B **43** 9938
[22] Broser I, Hoffmann A, Heitz R and Thurian P 1991 *J. Lumin.* **48+49** 693
[23] Kikoin K A and Fleurov V N 1994 *Transition Metal Impurities in Semiconductors. Electronic Structure and Physical Properties* (Singapore: World Scientific)
[24] Ham F S 1965 *Phys. Rev.* A **148** 1727
[25] Monemar B, Lindefelt U and Chen W M 1987 *Physica* B **146** 256
[26] Abragam A and Bleaney B 1970 *Electron Paramagnetic Resonance of Transition Ions* (Oxford: Clarendon)
[27] Yamaguchi T and Kamimura H 1972 *J. Phys. Soc. Japan* **33** 953
[28] Rashba E I and Gurgenishvili G E 1962 *Sov. Phys.–Solid State* **4** 759
Rashba E I and Gurgenishvili G E 1974 *Sov. Phys.–Semicond.* **8** 807
[29] Heitz R, Hoffmann A, Thurian P and Broser I 1992 *J. Phys.: Condens. Matter* **4** 157
[30] Cardona M 1963 *J. Phys. Chem. Solids* **24** 1543
[31] Rossler U 1969 *Phys. Rev.* **184** 733